In Situ Rutherford Backscattering Spectrometry for Electrochemical Studies

JES Focus Issue on Advanced Techniques in Corrosion Science in Memory of Hugh Isaacs

In Situ Rutherford Backscattering Spectrometry for Electrochemical Studies

M. Brocklebank,[1,z] J. J. Noël,[2,3,*] and L. V. Goncharova[1,3]

[1] *Department of Physics and Astronomy, The University of Western Ontario, London, ON, Canada*
[2] *Department of Chemistry, The University of Western Ontario, London, ON, Canada*
[3] *The Centre for Advanced Materials and Biomaterials Research (CAMBR), The University of Western Ontario, London, Ontario N6A 5B7, Canada*

A new in situ ultra-high vacuum (UHV) electrochemical cell containing a liquid electrolyte solution and Ti working electrode was designed and constructed to perform Rutherford backscattering spectrometry (RBS), under controlled electrochemical potentials. The depth resolution of RBS allowed for the determination of depth profiles for Ti, O, and other key transported species, in the electrode and in near-surface regions. Upon biasing the Ti electrode, subsequent RBS spectra releveled the time evolution of elemental depth profiles, characteristic of anodization, with Ti, O and Cl being mobile species. The differences between in situ and ex situ RBS measurements are emphasized. This work demonstrates the potential for in situ RBS to become a powerful tool for the investigation of a wide range of electrochemical processes including oxidation, electromigration, and deposition in batteries and other devices.
 [DOI: 10.1149/2.0301911jes]

Manuscript submitted March 25, 2019; revised manuscript received May 7, 2019. Published May 28, 2019. *This paper is part of the JES Focus Issue on Advanced Techniques in Corrosion Science in Memory of Hugh Isaacs.*

Developing corrosion resistant films and materials is grounded in a description of the fundamental mechanisms of oxidation, at the level of individual ionic species and their transport mechanisms. To gain insight into electrochemical processes on the atomic scale, it is necessary to create flexible, high-resolution, depth profiling techniques, which probe the fundamental constituents and describe their interactions with the greatest fidelity. Reactive metals such as Ti are of special interest, since, when exposed to oxygen rich environments, they spontaneously form oxides that are thermodynamically stable and highly insoluble, and hence provide excellent oxidation resistance in most media.[1]

While some physical properties of materials can be inferred from electrochemical measurements during anodization, many properties must be directly determined by in situ techniques, which probe the electrode, polarized at a controlled potential. In situ experiments are challenging to design, due to the liquid nature of the electrolyte solution. However, these in situ methods should (a) provide a range of surface-compositional and structural information, on a time scale that is commensurate with the electrochemical process, and (b) be compatible with geometric constraints of the process and the required temperatures and pressures. Ideally, these methods should also be non-destructive and have a high sensitivity. The development of numerous in situ electrochemical diffractometric and spectroscopic techniques[2–4] has expanded our understanding of the electrode-electrolyte interface. Techniques such as in situ X-ray diffraction (XRD) allow for the detection of crystalline phases,[5] in situ Fourier-transform infrared spectroscopy (FTIR)[6] and in situ X-ray photoelectron spectroscopy (XPS)[7] can provide information on chemical bonding, and in situ scanning tunneling microscopy (STM), can provide topographical information about an electrode's surface.[8]

As a complement to the abovementioned techniques, it is important to determine depth distributions of key major and minor elements present in the electrode and at the electrode/electrolyte interface. Rutherford backscattering spectrometry (RBS) is a rapid, non-destructive technique[9] in which a beam of mono-energetic ions is incident on a target, resulting in a small fraction ($\sim$ 0.01%) of those ions undergoing elastic collisions, due to repulsive Coulombic interactions with atomic nuclei. A fraction of these ions will backscatter in the direction of the detector, where the energy distribution of the backscattered ions is analyzed.

There are three properties of ion-matter interactions, which make RBS useful for quantitative depth profiling, yielding elemental areal density as a function of depth.[10] First, by assuming the collision between the incident ion and target atom is elastic, and by evoking conservation of energy and momentum, the energy of the backscattered ion (i.e. after the collision), is a function of the target atom's mass and the scattering angle (the latter is fixed by the detector's position). From this mass-dependence of the backscattered ion's energy, we can infer the element of the target atom. Second, the backscattering intensity, associated with a given element, is a linear function of the density of scattering centers, of that given element in the target (accuracy up to 3–5%) and so the integrated intensity of elemental RBS spectra can be used to infer elemental areal density. Third, for any given combination of incident ion, incident energy, and target composition, there will be a characteristic rate at which ions lose energy, as they penetrate, a given depth, into a target. By using this characteristic energy loss, one can convert measured energy losses experienced by the incident ions, into a corresponding depth penetrated. It is from this last property, that the widths of elemental RBS spectra can be used to infer into film thicknesses.

RBS can be used to determine the average stoichiometry over a depth of several hundred nanometers, with a fair depth resolution ($\sim$10 nm in the near surface region). This potentially allows for measurements of the areal density of elements in electrical double layers and near-surface layers of electrodes, formed during anodization.

RBS requires an ultra-high vacuum (UHV), which may confound the interpretation of some ex situ measurements, as transfer of electrodes from ambient conditions to UHV may result in compositional changes.[11] For example, the outermost layer may dehydrate; different intermediate phases may decompose, causing hydroxides to become oxyhydroxides and oxyhydroxides to become oxides;[12] or perhaps film thickness might be modified, due to these and related processes. For in situ RBS to be utilized to study electrochemical interfaces under potentiostatic control, it must overcome the challenges of working with a liquid electrolyte solution in UHV.

In situ RBS requires the use of an electrochemical cell that separates the liquid electrolyte solution from the UHV. This cell is placed in the UHV, and incident ions penetrate through a thin or ultra-thin window[13-16] (of Si or SiN, for example), to reach a metal electrode that has been deposited on the front of the window, which is in contact with the liquid electrolyte solution in the cell. If we bias the metal with respect to a reference electrode embedded in the cell, the deposited metal film serves as a working electrode to drive

*Electrochemical Society Member.
[z]E-mail: mbrockle@uwo.ca

electrochemical reactions, such as anodization. During anodization, incident ions backscatter from the metal/oxide and oxide/electrolyte interfaces and then pass (back out) through the SiN window, to reach the detector. Through changes in subsequent RBS spectra, the time evolution of the metal film's composition can be observed. Thin and ultra-thin Si and SiN windows are used due to the low atomic number (low-*Z*) of the element from which the window is composed and available through well-established fabrication procedures, using anisotropic chemical etching.[17]

In situ RBS was originally demonstrated by Kotz et al. who used 2.5 - 3 MeV He^+ beams passing through ≈1.2 μm Si windows.[14] Kotz emphasized the need for low-*Z* elemental windows, to avoid overlap of the signal originating from the electrode/electrolyte interface, and that originating from the Si window. In RBS, the probability of an incident ion backscattering from an atom is known as the scattering cross section and is proportional to Z^2 of the target atom. If the elements of interest are of lower-*Z* than Si (e.g., O), and if the widow is thick, the peaks corresponding to the element of interest will be obscured by the larger backscattering intensity of the substrate. Secondly, the authors[14] highlighted the phenomena known as energy straggling, whereby incident ions stochastically lose energy as they penetrate a target, resulting in a broadening of the (once) monoenergetic beam, and point out that this leads to degradation in depth resolution. These challenges can be overcome by minimizing the low-*Z* window's thickness or by using a single crystalline window through which the incident ions can be channeled.

Other in situ RBS studies have been performed with different window thickness to study various electrochemical systems. Forster et al. used ≈1 μm thick Si[15] windows and Morita et al. report using a Si thickness of 5.5 μm.[16] Most recently, Hightower et al. performed in situ RBS on 10 nm polycrystalline Au electrodes, deposited on a 150 nm thick Si_3N_4 windows.[13] They reported the ability to measure the diffuse double layer, electrode surface and near surface regions, and upon application of a negative polarization, they witnessed the formation of an iodide layer and the dissolution of the Au electrodes.

Previously reported in situ backscattering designs incorporated Si windows with thicknesses between 1 and 3.5 μm. Until now, the thinnest window reported for in situ RBS, by Hightower et al., was 150 nm thick. We used 100 nm-thick SiN windows to reduce the energy straggling and decrease the backscattering signal from the window. Thinner SiN windows were tested and were found not suitable for our studies, due to poor mechanical strength and a high failure rate. Additionally, most previous studies used larger energies, between 2 and 3 MeV. These high energies were necessary to penetrate the large thicknesses of the windows reported. In RBS, the scattering cross section has an E_0^{-2} dependence (where E_0 is the incident ion energy) and the 1 MeV we used for in situ RBS is advantageous to maximize the scattering cross sections and minimize the acquisition time for each consecutive RBS scan. By maximizing the number of scans in a given time interval, we intended to enable observation of more subtle changes to the electrode structure.

Experimental

The design of the electrochemical cell for in situ RBS analysis is shown in Figure 1. Design drawings were created in SolidWorks, and Western University Physics and Astronomy Machine Shop fabricated the cell. The area analyzed was limited by the dimensions of the He^+ beam, which was collimated by adjustable beam slits to 0.5 × 0.1 mm^2 or slightly smaller. The size of the SiN window was chosen to be of comparable dimensions. The 0.5 × 0.5 mm^2, 100 nm-thick SiN window, was centered on a 5 × 5 mm^2, 200 μm-thick, Si wafer. The windows are commercially available from Norcada and manufactured using standard etching techniques. The SiN window must be thin enough to allow the He^+ beam to traverse it entirely with minimal energy straggling and thick enough to withstand the pressure difference between the electrolyte in the cell and the UHV. The window and surrounding components must be composed of low-*Z* elements to prevent their backscattering intensity from obscuring the signal from the elements in the films below them (i.e., the oxide, metal, and electrolyte solution).

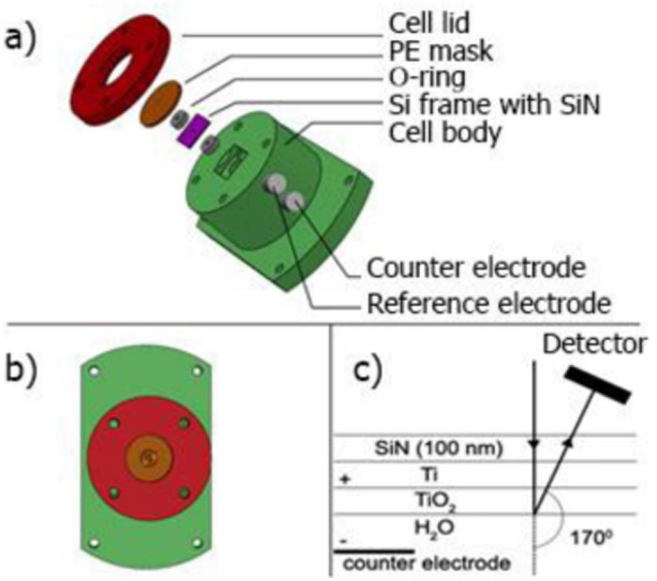

Figure 1. a) An exploded view of the electrochemical cell for in situ RBS. The Si frame with a 0.5 × 0.5 mm^2, 100 nm thick SiN window and a 60 nm thick layer of Ti deposited on it was centered inside the cell, b) the assembled view of the cell, from the top and c) the experimental geometry of the cell in the UHV system showing the direction of the incident ions (0°), and the scattering angle (θ = 170°).

The working electrode was a 40 – 60 nm-thick Ti layer that was magnetron sputtered onto the SiN window and is easily replaced after each experiment. The cell body and lid were constructed from polytetrafluoroethylene (PTFE), because of its UHV compatibility and low-reactivity with the potentially corrosive electrolyte. The liquid electrolyte solution was contained within the cell body and sealed by the first silicone O-ring. The Si wafer was placed between the first and second silicone O-rings to minimize stresses introduced by clamping the cell together. The PTFE lid and polyethylene (PE) mask were screwed into the cell with sufficient pressure to seal the first O-ring, without mechanically stressing or shattering the Si wafer. The PE mask was used as an aperture to further collimate the beam and prevent any contributions to the RBS spectra from the Si wafer. Electrochemical experiments employed three electrodes, with the Ti deposited on the window acting as the working electrode (WE), a Pt wire as the counter electrode (CE), and an AgCl-coated Ag wire as the reference electrode (RE). The RE and CE were embedded into the electrochemical cell body and sealed with Torrseal.

To facilitate data interpretation for the functional cell, preliminary simulations of the expected RBS spectra of the assembled cell ($SiN/Ti/H_2O$) were performed and are presented in Figure 2 (1 MeV He^+ ions, an incident angle of 0^0, and detector angle $\theta = 170^0$). Cl and Na were included because they were present at a concentration of 0.3 M in the electrolyte solution. Note that the cross section of H is too small for RBS to be sensitive to it. Before anodization (Figure 2a), 1 MeV He^+ ions are sufficiently energetic to provide good separation between elements, despite them having to pass through the entire 100 nm SiN window to reach the Ti. There is a degree of overlap between the backscattering signal from N in the window and O in the electrolyte solution, but the ≈ 30% larger cross section of O, tends to dominate. In Figure 2b, 50% of the Ti is oxidized, and this is reflected in the movement of the low-energy Ti edge position, toward lower energy, and a simultaneous decrease in backscattering yield from Ti in the oxide, given the linear proportionality between yield and elemental areal density. The thickness of 60 nm of Ti was chosen because thicker Ti films would lead to more overlap between the Si signal (from

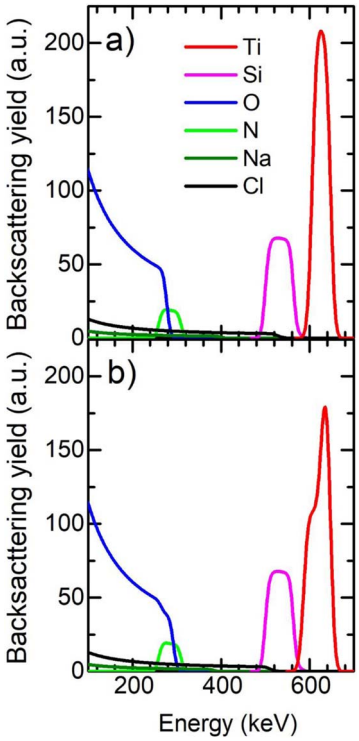

Figure 2. SIMNRA simulation of the expected RBS spectra associated with the assembled cell using 1 MeV He ions, incident angle of 0°, and θ = 170°, a) before anodization and b) after 50% of the Ti is oxidized.

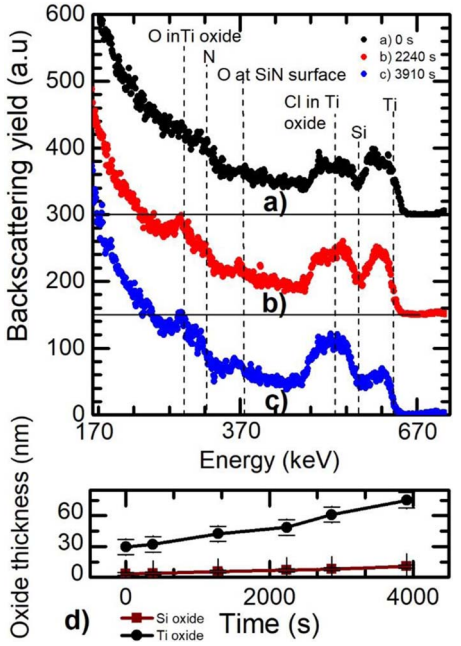

Figure 3. The time evolution of RBS spectra acquired with 1 MeV He^+ when Ti is biased at +2 V vs. Ag/AgCl (3 M Cl^-), for the times: a) 0 s (before bias), b) 2240 s, c) 3910 s. Horizontal lines represent the vertical offsets and dashed vertical lines represent the energy corresponding to the indicated element's initial edge position before polarization is applied, d) oxide thickness as a function of time for the Si oxide growing at the SiN/vacuum surface and the Ti oxide growing on the Ti electrode.

the window) and the Ti signal from the oxide as it thickened during anodization.

The linear tandem accelerator at the Tandetron Lab at Western University (1.7 MV, High Voltage Engineering Europa) was used to produce the He^+ ions for RBS. The backscattered He^+ energy distribution was measured with a surface barrier silicon detector (Ortec). The detector was located at a scattering angle of θ = 170° with respect to the direction of the incident beam, in "Cornell" geometry. The energy resolution of the detector was 12 keV, with a detector aperture of 2.0 mm × 6.1 mm. Simulated RBS energy distributions were generated using SIMNRA 6.06[18] software. The ion dose (in μC) was measured using a Faraday cup, which was moved periodically (1 s for every 4 s interval), to block the beam and probe the ion beam current. A high-precision 4-axis manipulator allowed for *x*-*y* translations of the samples in the RBS chamber within ± 0.05 mm. Consecutive *x*-*y* RBS scans were used to align the beam, normal to the SiN window surface. Electrochemical potential differences were applied, and currents were measured, with an AFCBP1 bipotentiostat (Pine Instrument Company), working in single potentiostat mode.

Results

Figure 3a shows the evolution of the RBS spectra when the Ti was biased potentiostatically at +2 V with respect to the Ag/AgCl RE in a 0.3 mol/L NaCl electrolyte. Individual RBS spectra were acquired using a 1 MeV He^+ beam, with a total dose of 0.25 μC per spectrum. Given the fluctuations in the beam current, the acquisition times varied between 5 and 6 min (300–360 s) per spectrum. The vertical dashed lines represent the high-energy edge position of the indicated element, which corresponds to the depth into the target that that element is initially found, before bias is applied. For example, for Ti this would be the Ti/SiN interface, at 629 keV. In RBS, the width of the spectral feature is linearly proportional to the physical thickness of the film and so the width of the Ti peak is consistent with the deposited Ti film thickness.

Experimental RBS spectra are convolutions of individual elemental spectra. By fitting the spectra in Figure 3 using SIMNRA, the contributions from each individual element can be isolated. Breaking the target into a series of sublayers, whose composition and thickness can be controlled, allows one to simulate RBS spectra, until the simulated and experimental spectra match, within experimental uncertainty. In Figure 4, the depth profiles used to simulate the RBS spectra for the times a) 0 s, b) 2240 s, and c) 3911 s are shown, and the resultant time evolution of the respective Cl, O and Ti elemental spectra are presented in Figure 5. In Figure 4, the break in the horizontal axis was included because this is the location of SiN, where the concentration of the indicated elements is zero. The O profile at the surface is part of a SiO_2 layer at the vacuum/SiN interface and the O at greater depths represents the growing TiO_x layer.

In RBS, the characteristic signs of Ti anodization (oxidation) include a decrease in Ti intensity at the low-energy Ti edge and simultaneously, an increase in O intensity at the high-energy O edge. As the oxide thickens, the width of the O feature grows monotonically toward lower energies (with an intensity that reflects O's stoichiometry in the oxide), and the width of RBS feature corresponding to the metallic Ti, becomes increasingly narrow, while the feature corresponding to Ti in the oxide, grow monotonically toward lower energies (with an intensity that reflects Ti's stoichiometry in the oxide). These effects can be observed in the sequence of RBS spectra shown in Figures 3–5. From 378 s to 2240 s, there is a decrease in Ti intensity around 589 keV and below, which occurs because the RBS yield is linearly proportional to the number of scattering centers of a given element, and the drop in Ti intensity corresponds to the lower Ti areal density in the oxide, relative to metallic Ti. Figure 5d shows that the total integrated Ti areal density remains relatively constant, indicating no significant Ti dissolution into the electrolyte solution (the lower Ti areal density at longer time scales will be addressed later). There is a concomitant increase in O at 267 keV, corresponding to oxide growth at the metal/oxide interface. From 2240 s to 3911 s, the growth of the O feature appears to increase to both higher (∼357 keV) and lower energy (287 keV and

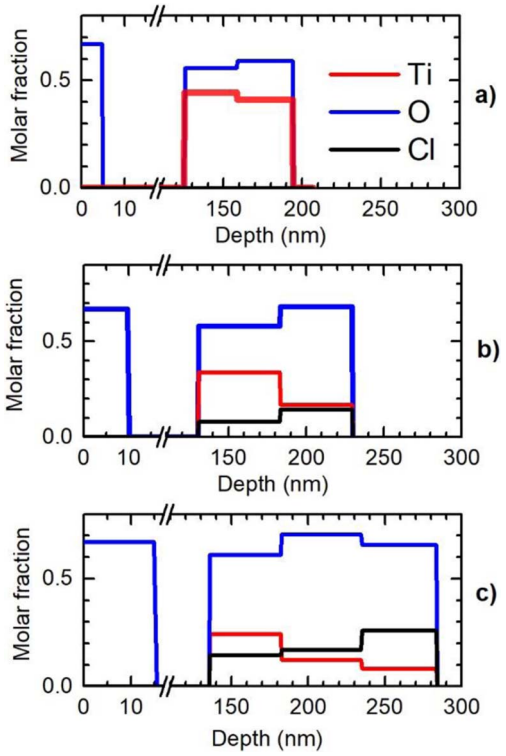

Figure 4. The depth profiles used to simulate the spectra in Figure 3: a) 0 s, b) 2240 s, c) 3911 s. The black line corresponds to Cl, the red to Ti, and the blue to O mole fraction. The depth axis has different scales before and after the break. The resultant individual elemental RBS spectra derived from these profiles are presented in Figure 5.

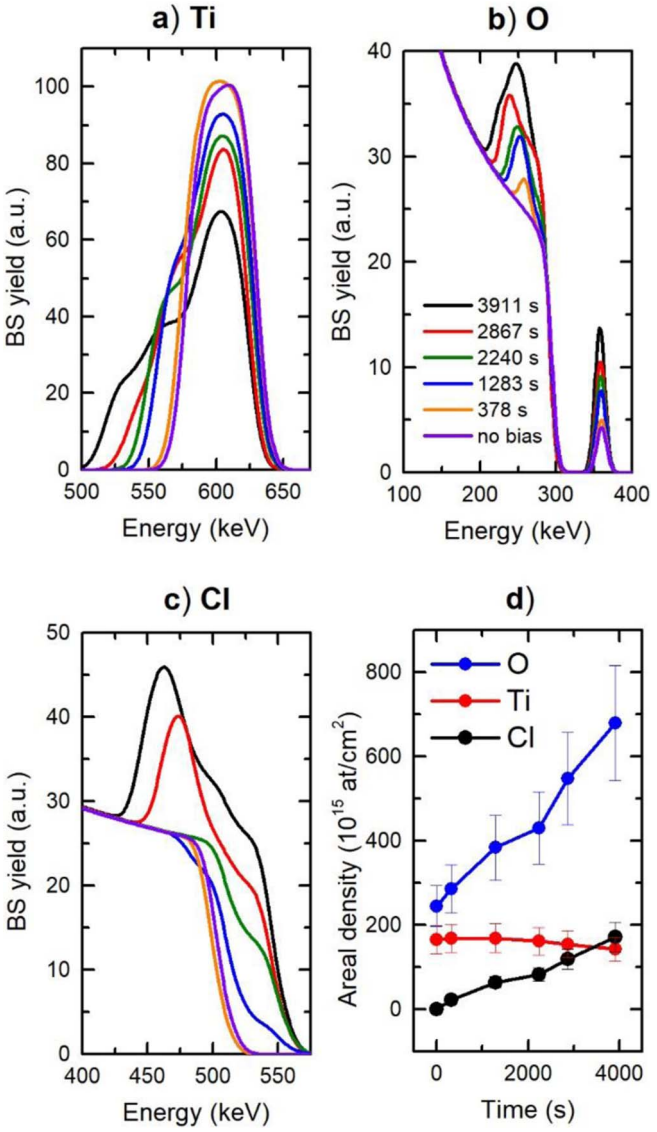

Figure 5. The time evolution of the spectra of individual elements a) Ti, b) O, and c) Cl, for the period 0 s - 3911 s, after simulating data with SIMNRA,[18] d) shows the total areal density of each element as a function of anodization time.

below) and the Ti signal is distributed over increasingly wider depths (toward lower energy relative to its positions at 330 s). The evolution of these two features corresponds to the continual growth of the Ti oxide over time.

With no bias applied, the passive oxide is free of chlorine but at 1283 s, the presence of Cl in the oxide adjacent to the Ti metal can be clearly observed, and the Cl concentration increases monotonically over time. At 3911 s the Cl is distributed throughout the entire Ti oxide film, with the highest concentration in the region adjacent to the oxide/solution interface. Growth of the oxide layers both at $H_2O/TiO_2/Ti$ interfaces and SiN/SiO_2/vacuum regions will be discussed in detail in the discussion section below.

In order to see what changes might occur in the films upon their transfer from ambient conditions to vacuum, the sample oxidized in situ was removed from the cell and measured with RBS using 2.5 MeV He^{++}, with the TiO_2 layer now facing the beam. A higher energy was selected to separate the Ti and Cl peaks. Figure 6a displays the ex situ RBS spectrum of an as-deposited 60 nm Ti film on 100 nm SiN and Figure 6b shows the spectrum of the Ti anodized at +2 V with respect to the RE. Note that the orientation of the Ti/SiN layers with respect to the incident beam was reversed for these spectra compared to those shown in Figures 3 – 5. Figure 6c shows the same experimental data as in b) but overlaid with the simulated spectrum that was used to fit the in situ spectrum from 3911 s, using the same experimental parameters as in a) and b).

Discussion

The RBS spectrum of the unoxidized sample in Figure 6a was fit by an integrated Ti areal density of $(2.5 \pm 0.1) \times 10^{17}$ atoms/cm^2, and the anodized sample in Figure 6b was fit by an integrated Ti areal density of $(2.7 \pm 0.1) \times 10^{17}$ atoms/cm^2. They agree within 9%, which is lower than the uncertainty associated with determination of the areal density (10%). However, the in situ Ti RBS spectra in Figure 4a were fit with $(1.7 \pm 0.1) \times 10^{17}$ atoms/cm^2 at 378 s, which decreases to $(1.4 \pm 0.1) \times 10^{17}$ atoms/cm^2 at 3911 s. As shown in Figures 6c, this is a significant decrease in Ti areal density relative to the ex situ RBS. Much of this difference is probably due to an imperfect alignment of the 0.5×0.5 mm^2 SiN window with respect to the incident beam when the cell is assembled. If the beam is not properly aligned relative to the SiN surface, then the Ti intensity will be adversely affected. The spectra in Figures 6a and 6b were taken with a beam incident on Ti that had been deposited over the entire 5×5 mm^2 SiN surface, and as such suffers no alignment problem.

The Pilling-Bedworth ratio, $\Re_{PB}$, is the ratio of the volume of the oxide, to the volume of the metal consumed in its production.[19] The distance that the metal/oxide interface moves inward (also the thickness of the metal consumed) is f_i and the distance the oxide/electrolyte moves outward is f_o. These are used to calculate the Pilling-Bedworth ratio:

$$\Re_{PB} = \frac{f_i + f_o}{f_i} = 1 + \frac{f_o}{f_i} \quad [1]$$

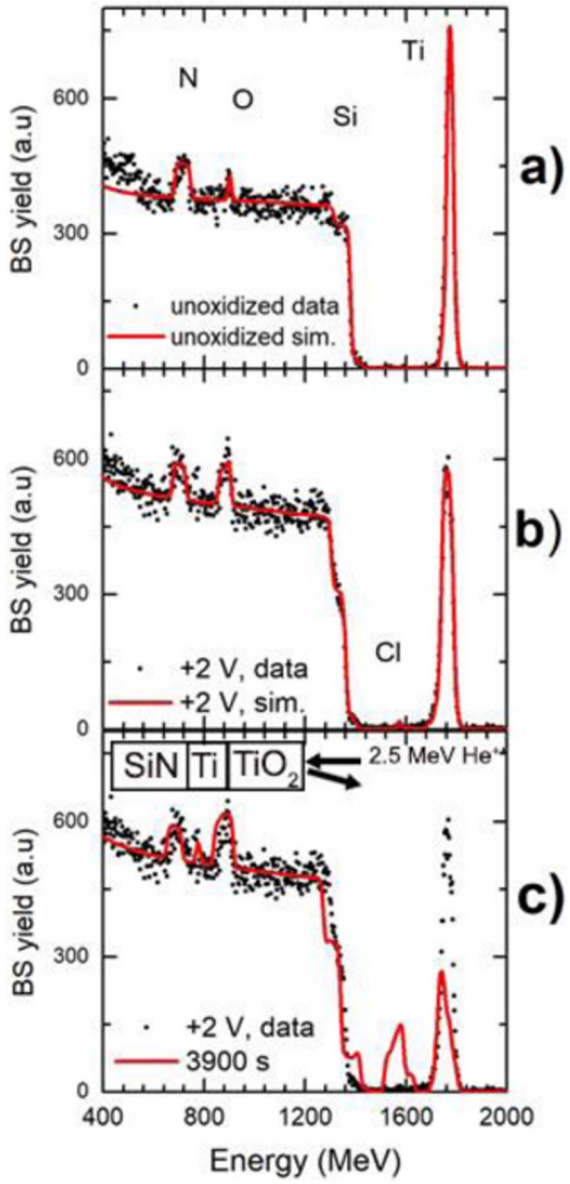

Figure 6. RBS spectra acquired with 2.5 MeV He^+ on a) unoxidized 60 nm Ti, b) the Ti oxide film that resulted from anodization at +2 V, and c) the same experimental data as in b) but overlaid with the simulated in situ spectrum after 3911 s of anodization.

Assuming 80% bulk densities, relative to the SiN/Ti interface, the metal/oxide interface moved inward by f_i = 37.0 nm and the oxide/electrolyte interface moved outward by a distance of f_o = 22.5 nm yielding $\Re_{PB}$ = 1.61. Assuming 100% bulk densities, f_i = 46.5 nm and f_o = 27.6 nm, yielding $\Re_{PB}$ = 1.59. The expected values are 1.77, 1.82, and 1.96 for rutile, brookite, and anatase respectively. The observed $\Re_{PB}$ suggests the anodic oxide is more dense than rutile, which may be the case for a thin amorphous film.

The anodization ratio, α, is the ratio of the thickness increase of the anodic oxide film to the increase in applied potential.[20] For a given metal such as Ti, α is constant for a given set of anodization parameters and over a rage of applied potentials.[21,22] According to the ex situ RBS results, the oxide layer thickened from 10.5 to 53.0 nm. The observed anodization ratio is α = (530.0 – 105.0 Å)/(2 V) = 213.0 $ÅV^{-1}$, which is not in good agreement with literature values, including 25.4 $ÅV^{-1}$ as determined by in-situ neutron reflectometry for Ti electrodes in aqueous NaCl solution,[23] 23.4 $ÅV^{-1}$ determined by Khalil and Leach using α spectrometry,[24] nor our own observed value of 24.5 ± 0.6 $ÅV^{-1}$ determined by ex situ medium energy ion scattering (MEIS) (to be published).

The observed α is almost an order of magnitude too large. If one assumes the value derived using MEIS and other methods is correct, to reach the final thickness reported here would require an applied potential of 25.3 V. While this calculation does not provide the exact potentials operative during anodization, it does suggest that the processes observed during in situ RBS were driven by larger fields than those that would result from the +2 V applied between the Ti WE and the Ag/AgCl RE. This may be a manifestation of charge accumulation, as the result of large amounts of incident positive He^+ ions accumulating in the insulating cell components, which could have generated a positive potential that greatly exceeding the potential applied by the potentiostat.

A competing explanation for the large experimental anodization ratio could be related to radiolysis effects, induced by energetic incident ions. The following mechanism has been given to account for the chemical effect of radiation:[25]

$$H_2O \rightarrow H_2O^+ + e^- \quad [2]$$

$$H_2O + e^- \rightarrow H + OH^- \quad [3]$$

$$H_2O^+ + H_2O \rightarrow H_3O^+ + OH \quad [4]$$

The free radicals would also react with one another to form H_2, O_2, and H_2O_2. It was reported by Kim and Oriani,[26] that Ti in brine solution under γ irradiation undergoes Ti corrosion caused by radiolysis products and not due to the radiation itself. They suggest that H_2O_2 is of particular importance as it provides another cathodic reaction (H_2O_2 reduction), and in their experiments, γ radiation resulted in thicker oxide layers than expected as a result of an applied potential alone. It has been observed that exposure of water to heavy-ion beams can also result in the same species[27] given in Equations 2 to 4, which might have contributed to or even dominated Ti oxide growth.

Figure 5c, shows that before a bias is applied, the initial passive oxide is free of Cl. There is only backscattering from the Cl^- in the electrolyte (Cl bulk signal begins at 508 keV). At 387 s, despite oxide growth having occurred, the oxide film is still free of Cl. At 1283 s, the presence of Cl can be detected in the oxide and the Cl mole fraction increases monotonically to 0.12 at 2240 s and reaches 0.14 at 3911 s, in the oxide layer directly adjacent to the Ti metal. At 3911 s, the outermost layer adjacent to the oxide has a Ti mole fraction of 0.08 and Cl mole fraction of 0.26, suggesting this is not an oxide region, but (partly) an aqueous phase, given the very low Ti areal density. The movement of the Cl edges to both higher and lower energy possibly suggests that Cl^- ions are entering the oxide as interstitials and are migrating inwards in response to the direction of the bias.

However, given the depth resolution of RBS, it is difficult to fully determine the layered composition of the electrode in greater detail. The Cl peak overlaps with the signal originating from the Si in the SiN window, and the interference becomes worse at longer time intervals, as there is additional overlap with the signal from Ti as it moves to lower energies during oxide growth. Ultimately, it is difficult to determine how the Cl high-energy edge changes and the depiction of it moving toward higher energy (i.e., toward the metal/oxide interface), as in Figure 5c, might be inaccurate.

During anodization, more Cl was present in the oxide than was observed with ex situ RBS. Even if the Cl content was overestimated, for reasons discussed above, transfer of the oxide film from the ambient environment to the UHV resulted in significant Cl loss. Figure 6b only indicates a Cl mole fraction of 0.05 in the first 27.5 nm of the oxide. The loss of Cl may support the claim that the Cl is incorporated into the oxide without breaking Ti-O bonds, as discussed above. The Ti-Cl bond dissociation energy is 507 kJ/mol and that for Ti-O is 673 kJ/mol, which explains why Ti-O would be preferentially formed. Even if Ti-Cl bonds are formed, it is favorable to convert Ti chloride to TiO_2 via

hydrolysis:

$$TiCl_4 + 2H_2O \rightarrow TiO_2 + 4HCl \quad [5]$$

SiO_2 growth.—According to the RBS spectra in Figure 3, there is a spectral feature around 367 keV that grew monotonically over time and whose high-energy edge position remained unchanged. From the depth profiles in Figure 4, this was simulated as O in a SiO_2 layer at the SiN/vacuum interface. Using 80% bulk density during simulations, the observed SiO_2 thickness was initially 4.8 nm, with no bias, and increased to 15.7 nm after 3911 s at +2 V vs. Ag/AgCl (3 M Cl^-). Also note, in the ex situ RBS measurements of the anodized film (Figure 6c), there is a second O peak corresponding to this SiO_2 layer that is consistent with a thickness of 15.7 nm.

The in situ RBS spectra are consistent with simulated parameters that describe the SiN layer as decreasing in thickness from 97 ± 1 nm at no bias, to 92 ± 1 nm after 3911 s. This reduction in SiN thickness results in a Si areal density decrease of $(20.0 \pm 0.1) \times 10^{15}$ atoms/cm^2, while the increase in Si areal density as the SiO_2 layer thickens is $(23.3 \pm 0.1) \times 10^{15}$ atoms/cm^2. The most likely source of Si in the SiO_2 layer is the consumption of the SiN layer.

It is feasible that O could come from the vacuum. The impingement rate, Ω, for H_2O in the UHV can be calculated by:

$$\Omega = \frac{P}{\sqrt{2\pi k_B T m}} \quad [6]$$

where k_B is Boltzmann's constant, m the mass of the molecular species in the vacuum, P the pressure, and T the absolute temperature. For H_2O at 300 K, a pressure of 1.33×10^{-4} Pa (10^{-6} torr), and assuming a sticking coefficient of $\sigma = 0.1$, the rate at which water molecules both impinge on the surface and adhere to it is 4.8×10^{13} cm^{-2}s^{-1}. A 15.7 nm thick SiO_2 layer would have 6.7×10^{16} O atoms, which, given the assumed sticking rate, would require 1.4×10^3 s to accumulate. The elapsed time in our experiments was ∼ 280% of that required time, so it is not unreasonable to suggest that all the O atoms present in the SiO_2 layer might have come from the vacuum. However, the sticking coefficient is probably overestimated. It is also possible that the local pressure could have been much higher in the presence of a microscopic leak around the location of the window. It is unlikely that the SiO_2 layer thickening from 4.8 nm to 15.7 nm was a spontaneous process and a source of energy was required to facilitate these chemical reactions. Most likely, the ion beam was driving radiolysis.

Note that from present observations alone, it is not possible gain exact insight into the underlying anodic oxide growth mechanisms. The movement of the in situ RBS O features (Figure 5b), toward both higher and lower energy represents the continual growth of the Ti oxide. The movement of the O features is consistent with a number of explanations: *(i)* transport of O to, and oxide growth at, both the oxide/solution and metal/oxide interfaces simultaneously, *(ii)* growth at a single interface (oxide/solution or metal/oxide), accompanied by the volume expansion, associated with Ti metal being converted into Ti oxide. Nor can we even preclude oxide growth occurring somewhere in the middle of the pre-existing oxide; although the authors know of no growth models which describe anodic oxide growth at these locations, this is, in principle, consistent with the RBS results. The time evolution of the Ti signal (Figure 5a) is also consistent with any of the above interpretations and contains no unique information.

In future experiments it would be possible to elucidate at which interfaces oxide growth is occurring during anodization by the use of the appropriate marker layer for reference. The in situ backscattering measurements reported here complement additional research done by the present authors (to be published), which are ex situ attempts to quantify the O elemental depth profiles in anodic Ti oxide films, as measured using nuclear reaction profiling (NRP) and MEIS in conjunction with an $^{16}O/^{18}O$ isotopic labeling procedure. One of the important conclusions is that oxide growth occurs at both the oxide/electrolyte and the oxide/metal interfaces, simultaneously. Similar isotopic labeling could be performed on the deposited Ti and incorporated in the electrochemical cell that is described in this paper.

Ion beam exposure effects.—Prior to applying an electrochemical bias to the Ti, preliminary RBS was performed to determine whether exposure to the ion beam alone led to compositional changes. Apparent movement of the high-energy Ti and Si edge positions to lower energy (∼10-15 keV) and reductions in Ti intensity (∼20–25%) were observed. The magnitude of the reduction in intensity and the shift in edge position effects were proportional to the total acquisition time (until the effect saturated at the values given above). Notably, after the ion beam was removed from the surface for a sufficiently long time, the original spectrum (without shifts) could be reproduced.

A possible explanation of the observed phenomena is charge accumulation on the surface of the cell. Given the insulating components, if a sufficiently large number of positive charges accumulated and established an electric field, this would repel incident ions and they would experience a degree of energy loss before backscattering, resulting in a shift in the incident energy. However, given the E^{-2} dependence of the differential scattering cross sections in RBS, lower energy incident ions might be expected to increase the backscattering intensity, which is not consistent with observation. Nor would it explain why only the Ti intensity seems to be affected.

Alternatively, the formation of a SiO_2 layer at the Ti/SiN interface, or some restructuring of this interface, induced by beam exposure, would explain the movement of the Ti edge toward lower energy and the fact that only the Ti features are impacted. This is unlikely, since the effect would have to be reversible.

Conclusions

An electrochemical cell has been designed, constructed, and tested using a 100 nm SiN window and a deposited 60 nm-thick Ti electrode layer. Upon biasing the Ti, with respect to the Ag/AgCl RE at +2 V in a 0.3 mol/L NaCl solution, characteristic features of anodization are observed in a series of RBS spectra taken over time. Cl incorporation most likely happens when Cl ions enter the oxide interstitially and subsequently migrate into the oxide, given the direction of the bias. There are compositional differences between the films observed by in situ and ex situ measurements; the Cl concentrations in the films observed by in situ measurements are much higher than those seen in *ezx situ* RBS measurements following anodization, implying Cl loss when exposed to UHV. Decreases in the expected Ti intensity were observed and explained in terms of poor alignment of the cell with respect to the ion beam and possible charge accumulation effects.

In situ RBS can be used to determine quantitative elemental depth profiles, on time scales commensurate with the anodization process. This is useful information, which complements the topographical, chemical, and structural information, provided from other in situ techniques. However, we have identified some clear limitations. In situ RBS requires a window to seal the electrolyte inside the cell. As incident ions penetrate the width of the window, the ions lose energy stochastically, resulting in a broadening of the initially monoenergetic beam. With ion beam techniques, the increasing uncertainty in the beam energy, translates to an increasing uncertainty in the depth being probed, i.e. degradations in depth resolution. To avoid such effects, it is imperative to minimize both the window thickness and the thickness of the deposited metallic layer.

Secondly, the window's contribution to the RBS spectra can be significant and can obscure other key elemental features. In the present study, the RBS features corresponding to deposited Ti and Si (in the window), where initially well separated. During oxidation, the movement of Ti features toward lower energies, led to an overlap with the Si signal. On even larger time-scales, the Cl incorporated in the oxide, at the oxide/electrolyte interface, resulted in RBS features that overlapped with both the Ti and Si at the same time. Such overlap, increases uncertainty when determining stoichiometry and layer thickness. Systems appropriate for in situ RBS are those in which the elemental features are well separated (i.e. large mass differences between elements),

and maintain that separation on both on short and long timescales. Also, there is always some difficulty studying low-Z elements, such as O (of clear significance when studying oxidation), which have small differential cross sections in RBS and low mass, which results in O features often being obscured by heavier elements in the system.

Lastly, in the present study, it is uncertain whether the high observed Ti anodization ratio, was a product of ion beam-driven radiolysis, as opposed to just the applied potential difference. Were this proven to be the case, it would be difficult to use the methods presented here, to study systems such as anodization. Note that Ti anodization has been studied using in situ neutron reflectometry (NR),[23] employing a similar electrochemical cell, as described in the present study. Given that the authors do not report any observed radiation effects, techniques such as NR might preferred to study metals anodization while avoiding radiation effects.

Acknowledgment

This research was supported by the Natural Sciences and Engineering Research Council of Canada and the Canada Foundation for Innovation. We would like to thank Jack Hendricks (Tandetron facility at the University of Western Ontario) for his help with data acquisition and Western Physics and Astronomy Machine Shop for the fabrication of the in-situ cell.

ORCID

M. Brocklebank https://orcid.org/0000-0002-3188-2451
J. J. Noël https://orcid.org/0000-0003-3467-4778

References

1. J. Lausma, L. Mattsson, U. Rolander, and B. Kasemo, *Mater Res. Soc. Symp. Proc.*, **55**, 351 (1986).
2. J. H. White, M. J. Albarelli, H. D. Abruna, L. Blum, O. R. Melroy, M. G. Samant, G. L. Borges, and J. G. Gordon, *J. Phys. Chem.*, **92**, 4432 (1988).
3. V. R. Stamenkovic, M. Arenz, C. A. Lucas, M. E. Gallagher, P. N. Ross, and N. M. Markovic, *J. Am. Chem. Soc.*, **125**, 2736 (2003).
4. X. F. Lin, B. Ren, and Z. Q. Tian, *J. Phys. Chem. B*, **108**, 981 (2004).
5. J. Wang, B. M. Ocko, A. J. Davenport, and H. S. Isaacs, *Phys. Rev. B*, **46**, 10321 (1992).
6. G. Lefèvre, *Adv. Colloid and Interface Sci.*, **107**, 109 (2004).
7. T. Fujii, F. M. de Groot, G. A. Sawatzky, F. C. Voogt, T. T. Hibma, and K. Okada, *Phys. Rev. B*, **59**, 3195 (1999).
8. K. Itaya, *Prog. Surf. Sci.*, **58**, 121 (1998).
9. W. K. Chu, J. W. Mayer, and M. A. Nicolet, *Backscattering Spectrometry*, Academic Press, Inc (1978).
10. C. Jeynes, Z. H. Jafri, R. P. Webb, A. C. Kimber, and M. J. Ashwin, *Surf. Interface Anal.*, **25**, 254 (1997).
11. E. Yeager, *Surf. Sci.*, **101**, 1 (1980).
12. D. D. MacDonald, *Electrochim. Acta*, **56**, 1761 (2011).
13. A. Hightower, B. Koel, and T. Felter, *Electrochim. Acta*, **54**, 1777 (2009).
14. R. Kotz, J. Gobrecht, S. Stucki, and R. Pixley, *Electrochim. Acta*, **31**, 169 (1986).
15. J. S. Forster, D. Philips, J. Gulens, D. A. Harrington, and R. L. Tapping, *Nuc. Inst. & Meth. Phys. B*, **28**, 385 (1987).
16. K. Morita, J. Yuhara, R. Ishigami, B. Tsuchiya, K. Soda, K. Saitoh, S. Yamamoto, P. Goppelt-Langer, Y. Aoki, H. Takeshita, and H. Naramoto, *Rad. Phys. Chem.*, **49**, 603 (1997).
17. K. E. Bean, *IEEE Trans. Electron Devices*, **25**, 1185 (1978).
18. M. Mayer, 1997.
19. N. B. Pilling and R. E. Bedworth, *J. Inst. Met.*, **29**, 529 (1923).
20. R. M. Torresi, O. R. Camera, C. P. De Pauli, and M. C. Giordano, *Electrochim. Acta*, **32** (1987).
21. D. Thwaites, *Nucl. Instrum. Meth. Phys. Res. Sect. B*, **27**, 293 (1987).
22. C. K. Dyer and J. S. L. Leach, *J. Electrochem. Soc.*, **125** (1978).
23. Z. Tun, J. J. Noël, and D. W. Shoesmith, *J. Electrochem. Soc.*, **146**, 130 (1999).
24. N. Khalil and J. S. L. Leach, *Electrochim. Acta*, **31**, 1279 (1986).
25. R. S. Glass, *Sandia Report No. SAND 81.1677*, (1981).
26. Y. J. Kim and R. A. Oriani, *Corrosion*, **43**, 92 (1987).
27. Y. Hatano, Y. Katsumura, and A. Mozumder, *Charged Particle and Photon Interactions with Matter: Recent Advances, Applications, and Interfaces*, CRC Press (2010).